# ELECTRODE DISINTEGRATION UNDER THE ACTION OF THE FLAME COMPONENT

N. V. Afanas'ev, S. N. Kapel'yan,
V. A. Morozov, and L. P. Filippov

UDC 537.523.4

We examine the disintegration of electrodes made of various metals, under the action of the flame component of a spark discharge. We calculate the flame velocity and the pressure within the discharge jet.

In the case of powerful pulse discharges, flames generated by the vapors of the eroded metal usually burst forth from the electrodes toward the surface, and the flame velocities are on the order of $10^3$-$10^4$ m/sec [1]. Exhibiting great kinetic and intrinsic energy, these flames are capable of melting, partially vaporizing, and expelling the molten metal from the surface of the opposing electrode. Depending on the conditions of the pulse discharge, the role of the flame mechanism in electrical erosion may be quite substantial [1-3]. It would therefore be of interest experimentally to evaluate the role of the gasdynamic factors at various discharge energies.

We investigated the erosion capacity of the cathode and anode flames ($\tau_W = 210 \cdot 10^{-6}$ sec, W = 20-900 J) for electrodes made of six different metals: Pb, Zn, Al, Fe, Cu, and W, with a constant distance between the electrodes. The flame was generated in accordance with the method described in [1] and directed at a fixed barrier. Electrode erosion and the erosion of the barrier were measured by weighing on a microanalytical balance and by comparison with the corresponding magnitude of erosion for coaxially mounted electrodes. The amount of material eroded from an aluminum barrier as a consequence of the anode (at the bottom) and cathode (at the top) flames at various discharge energies is given in Fig. 1.

With an increase in the energy stored in the capacitor bank from 20 to 900 J, the erosion of the barrier by the flame producing electrodes made of each of the metals under investigation increases virtually linearly. For the anode flame, a number of metals (Pb, Zn, Al, Fe, Cu, and W) differ substantially in terms of effect on an aluminum barrier from the metals for the cathode flame (Cu, Fe, Al, Zn, Pb, W). The extent to which the barrier is eroded by the anode flame discharging from the low-melting metals (Pb, Zn, Al) and W is greater by a factor of 1.8-3.3 and the corresponding quantity for the cathode flame. In the case of copper and iron electrodes, the destruction of the barrier as a consequence of the anode and cathode flames is virtually identical. It should be noted that beginning approximately with a discharge energy of 100 J (Table 1), the quantity $\Delta m_{fa}$ for the erosive action of the anode flame on an aluminum barrier and the quantity $\Delta m_{fc}$ of the cathode flame are so great that they exceed the erosion of corresponding

TABLE 1. Magnitude of Barrier Erosion as a Ratio of the Erosion of the Corresponding Flame-Producing and Coaxially Positioned Electrodes

| W, J | $\frac{\Delta m_{fa}}{\Delta m_a}$ | $\frac{\Delta m_{fc}}{\Delta m_c}$ | $\frac{\Delta m_{fa}}{\Delta m_{aX}}$ | $\frac{\Delta m_{fc}}{\Delta m_{cX}}$ |
|---|---|---|---|---|
| 900 | 4,9 | 4,9 | 1,3 | 1,1 |
| 400 | 5,7 | 5,1 | 1,1 | 0,9 |
| 144 | 7 | 6 | 0,9 | 0,7 |
| 36 | 1,5 | 1,5 | 0,2 | 0,05 |

Belorussian Polytechnic Institute, Minsk. Translated from Inzhenerno-Fizicheskii Zhurnal, Vol. 17, No. 1, pp. 43-49, July, 1969. Original article submitted September 27, 1968.

© 1972 Consultants Bureau, a division of Plenum Publishing Corporation, 227 West 17th Street, New York, N. Y. 10011. All rights reserved. This article cannot be reproduced for any purpose whatsoever without permission of the publisher. A copy of this article is available from the publisher for $15.00.

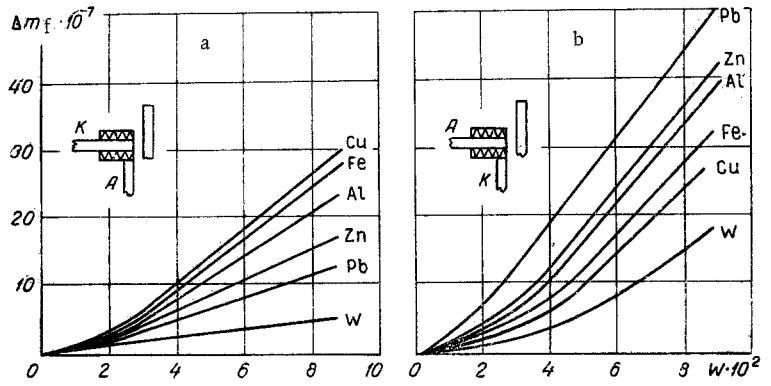


Fig. 1. Aluminum barrier erosion $\Delta m_f \cdot 10^{-7}$ kg as a function of the cathode (a) and anode (b) flames for various discharge energies $W \cdot 10^2$ J.

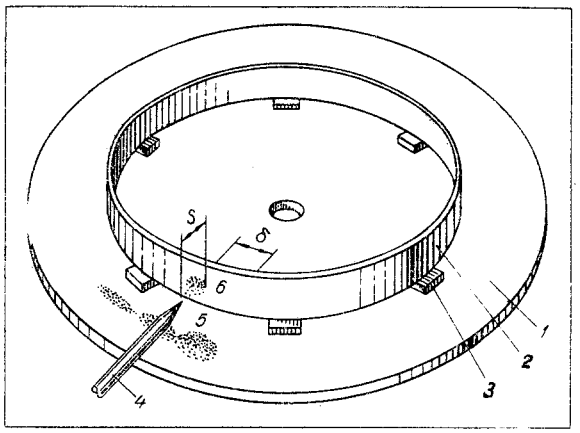


Fig. 2. Diagram showing the installation for a space–time scan of the tracks left by the flame and the discharge channel: 1) disc surface; 2) rim; 3) attachment and rim insulation; 4) fixed electrode; 5) discharge-track scan on the disc surface; 6) flame scan on the side surface of the rim.

aluminum flame-producing electrodes, i.e., $\Delta m_a$ and $\Delta m_c$, by a factor of 3-7, while exceeding by a factor of 1.0-1.3 the magnitude of the erosion for coaxially positioned aluminum electrodes, i.e., $\Delta m_{ax}$ and $\Delta m_{cx}$. The last indicates that a substantial fraction of the energy evolved in the discharge on the flame-producing electrode is dissipated by the high-temperature flames from the vapors of the eroded metal. The erosion of a nonflame-producing electrode (plates A and C in Fig. 1) is insignificant and for all of the metals under discussion it is smaller by an order of magnitude, and in certain cases smaller by two orders of magnitude than when the electrodes are coaxially positioned. In this case the migration area for the discharge channel on the surface of the nonflame-producing electrode is substantially larger than in the case in which the electrodes are coaxially positioned. Channel migration in spark discharges under the experimental conditions is indicated by the tracks left by the discharge channel on the surface of the nonflame-producing electrode for the anode and the cathode, respectively. On the anode this constitutes a collection of fine used depressions of regular shape, while on the cathode we observe the typical cathode tracks and the "branched systems," similar to those described in [3]. These results confirm the hypotheses with respect to the migrating channel [4, 5]. It should be noted that on separation of the discharge channel and the flame similar phenomena are regularly observed for all metals. If the discharge gap is sufficiently long we observe spatially separated microlunes and "branching" cathode tracks for the coaxially positioned electrodes as well. If the spark-discharge channel migrates over the surface of the electrode, the flame must exhibit a discrete structure.

To check this out, we set up a space–time scan of the flame and discharge-channel tracks (Fig. 2). The pulse discharge was achieved between the fixed electrode 4 housed in a quartz cube, and the surface of the rotating disc 1 which served as the opposite electrode. In this case, the flame impinged on the side surface of the thin-walled insulated rim 2 attached to the rotating disc. The track left by the discharge flame on the polished surface of the metal rim (Fig. 3a) forms a surface coated with a nonhomogeneous layer of vapors from the opposite electrodes (the dark coating). Against a dark background, we note numerous white spots of irregular shape, scattered randomly over the surface. A study of these tracks showed that they are elevated above the level surface and that they represent individual eroded portions of irregular shape. On the whole, this experiment permits us to draw the conclusion that the flame is a two-phase system consisting of individual clusters of high-temperature vapor, and these are responsible for the individual eroded segment on the rim, in addition to a liquid phase formed by the substance of the

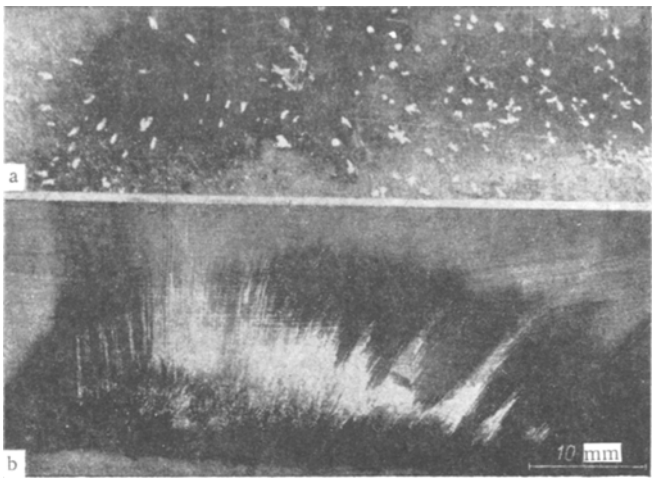


Fig. 3. Track left by the discharge flame on the surface of the rotating rim (a) and on the surface of the rotating disc (b).

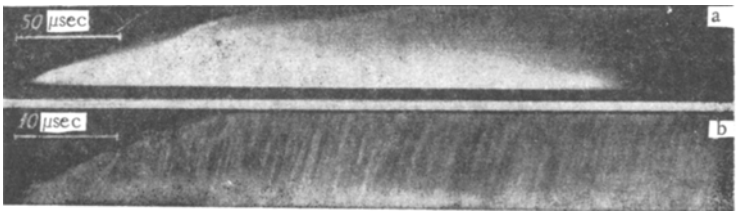


Fig. 4. Time scan of a spark-discharge flame by means of an SFR-2 camera for $q < q_{cr}$ (a) and $q > q_{cr}$ (b).

electrodes (the protuberances on the rim). This conclusion is confirmed by the flame-track scan directed at an acute angle to the surface of the rotating disc (Fig. 3b).

The time scan of a flame from a condensed spark discharge, accomplished with an SFR-2 camera, also shows that the flame actually consists of individual jets of high-temperature vapor (Fig. 4b) whose velocities are functions of the current density for the energy supplied. With a constant magnitude of the latter, the jet velocities are identical (Fig. 4b), and this indicates that the elementary processes proceed identically within each microlune of the electrode surface.

The migrating discharge channel spatially separated from the flame of the opposite electrode will cause the metal in the microlune region to vaporize intensively as a consequence of intensive heat liberation. In the one-dimensional formulation the thermophysical problem involving a surface heat source (which is valid for a discharge with current densities $j \leq 10^7 A/cm^2$ [6]) is formulated for a moving vaporization front whose coordinate origin is situated precisely at the vaporization front; this formulation is treated in [6, 7].

In analogy with [6, 7], assuming a Frenkel vaporization mechanism for the case under consideration, i.e.,

$$\frac{dn}{ndt} = \nu_0 e^{-\frac{U_0}{kT}}, \tag{1}$$

for the temperature T of the moving vaporization front we derive the following expressions:

$$T = \frac{\frac{r}{R} \lg e}{\lg v_0 - \lg v}, \tag{2}$$

$$v_0 = \frac{n_0'}{n_0} \nu_0. \tag{3}$$

TABLE 2. Theoretical Values for the Minimum Velocities of Jet Discharge

| Metal | Bi | Pb | Cd | Sn | W | Ni, Cu | Fe, Mg | Mo | Zn | Al |
|---|---|---|---|---|---|---|---|---|---|---|
| $U$, km/sec | 0,87 | 0,9 | 0,94 | 1,65 | 1,74 | 2,14 | 2,25 | 2,28 | 2,52 | 3,15 |

Assuming that the metal vapor subsequently forming into a plasma jet behaves as an ideal gas with a certain effective value for the adiabatic exponent $\beta$, for the vapor pressure at the instant of jet discharge we obtain

$$P = n_0 kTe^{-\frac{r}{RT}}. \tag{4}$$

Experiments show [7] that the initial discharge velocity for the plasma jet is virtually independent of the external pressure. To determine the initial velocity of the plasma jet we can therefore apply the theory of gas discharge from a vessel into a vacuum, with discontinuous opening of the barrier. In the case of nonsteady motion the discharge velocity U for the jet in this case is equal to

$$U = \frac{2c_0}{\beta - 1}, \tag{5}$$

where

$$c_0 = \left(\frac{\beta P}{\gamma_0}\right)^{1/2}. \tag{6}$$

Substituting the value of P from (4) and considering that – according to the Frenkel vaporization mechanism – the vapor density $\gamma$ in the jet is associated with the density $\gamma_0$ for the original metal by the relationship

$$\gamma = \gamma_0 e^{-\frac{r}{RT}}, \tag{7}$$

for the plasma-jet velocity U we derive the expression

$$U = \frac{2}{\beta - 1}\left(\frac{\beta n_0 kT}{\gamma_0}\right)^{1/2}. \tag{8}$$

It follows from (8) that the initial flame velocity and, consequently, its energy depends on T whose value for the various heat flows has been calculated in [6, 7]. As follows from [7, 8], with an increase in the discharge energy there is a rise in the energy current density, in the density of the vapor flow, and in its temperature, and this, in the final analysis, leads to an increase in the destructive capacity of the flame when it acts on a barrier. Assuming the metal vapor to be monoatomic and an ideal gas, we should assume that $\beta = 1.67$; however, with an increase in T, considering the processes of ionization and dissociation, the value of $\beta$ varies smoothly from 1.67 through 1.2-1.3 [8].

The values of the calculated minimum plasma-jet discharge velocities for the case in which $T = T_{boil}$ and $\beta = 1.67$ for a number of metals are given in Table 2.

The time scans of the flame, accomplished with the SFR-2 camera, actually demonstrates that the jet discharge of the vapor begins at some critical value for the heat-flux density which is different for the various metals. With a heat-flux density lower than the critical, individual jets are not found in the flame (Fig. 4a) and quiet evaporation takes place. With an increase in the theat-flux density (q) the velocity of motion for the vaporization front increases and when $q > q_{cr}$ we begin to observe individual metal vapor jets (Fig. 4b). The experimental values for the jet velocity at heat-flux densities slightly in excess of $q_{cr}$ are given in Table 3.

The satisfactory agreement between the data presented in Tables 2 and 3 makes it possible to assume that the vaporization assumes the nature of a jet and, consequently, that channel migration begins as soon as the electrode surface temperature in the discharge zone exceeds $T_{boil}$. The basic fraction of the eroded metal in this case, i.e., the erosion which results exclusively as a consequence of the discharge channel,

TABLE 3. Experimental Values of the Minimum Jet Discharge Velocities

| Metal | Cd, Pb | Mo, Sn | W, Cu | Fe | Al |
|---|---|---|---|---|---|
| $U$,km/sec | 1,0 | 1,55 | 2,2 | 2,8 | 3,0 |

must make up the vapor phase of the metal. Electrode erosion for the diagram shown in Fig. 1 is therefore so insignificant. For coaxial electrodes situated near each other, the area of channel migration over the surface is substantially smaller. We have an intensive compact plane composed of the ionized high-temperature vapor heated to the channel temperature within the discharge plasma. In this case, because of the flame component of the opposite electrodes, there is a mutual transfer of energy between the anode and the cathode. In addition to the vaporized metal, liquid metal appears in the erosion zone, and some quantity of this liquid metal is removed together with the electrodes under the action of the pressure pulses which are generated during the discharge process [9]. The gasdynamic forces which are generated as the high-speed vapor flow impacts against the surface of the fixed electrode play an important role in expelling the liquid metal from the discharge lune. Naturally, the magnitude of erosion for coaxially positioned electrodes is very much greater than for electrodes producing a flame that is separated through some distance from the channel.

It follows from this investigation that the isolated flame can produce erosion that is equal to or even larger than the electrode erosion in the case of coaxially positioned electrodes. This becomes understandable if we take into consideration that the action of the flame on the barrier is somewhat different than the effect of the flames on the electrodes when the latter are coaxially positioned. In the latter case the cathode and anode flames move toward each other, and they interact, which leads to a change in their energy state [10]. When the flame acts on the cold metallic barrier, the latter receives a substantial fraction of the flame energy, and this is the greater, the higher the flow velocity (U), the vapor density ($\gamma$) and the vapor temperature (T). It should be borne in mind that when the flame plasma strikes the cold metal surface there is partial (or perhaps complete) deionization of the plasma, which substantially increases the quantity of energy transmitted to the barrier. The magnitude of barrier erosion may therefore be of the same order of magnitude and may even exceed the erosion of the corresponding electrodes that are coaxially positioned. The destructive capacity of the flames produced by various metals, all other conditions being equal, is substantially different (there are differences in temperature, vapor-flow density, and vapor velocity). In addition, the processes at the cathode and anode are quite dissimilar [6], and this probably also affects the magnitude of the destructive capacity of the cathode and anode flames in the case of a different sequence of metals for a flame-producing electrode (Fig. 1). In this case we must take into consideration the specific nature of the pulse discharge and to examine from the theoretical standpoint the process of vapor formation, in a manner similar to the examination of the effect of a laser beam on metal.

## NOTATION

$\nu_0$ is the oscillation frequency of the surface atom about the equilibrium position;
$U_0$ is the potential energy of the particle on vaporization;
$dn/ndt$ is the probability of surface-atom vaporization per unit time;
$k$ is the Boltzmann constant;
$r$ is the specific heat of vaporization;
$v$ is the velocity of the vaporization front;
$R$ is the universal gas constant;
$n_0'$ and $n_0$ are the numbers of atoms per unit surface and per unit volume;
$c_0$ is the local speed of sound under corresponding thermodynamic conditions.

## LITERATURE CITED


1. S. L. Mandel'shtam and S. M. Raiskii, Izv. Akad. Nauk SSSR, Seriya Fizich., 13, No. 5, 549 (1949).
2. B. N. Zolotykh, in: Problems of Electric Spark Treatment of Metals [in Russian], Izd. AN SSSR 1960
3. I. G. Kesaev, Cathode Processes of a Mercury Arc and Problems of Its Stability [in Russian], Gosénergoizdat (1961).

4. N. V. Afanas'ev et al., in: Electrical Contacts [in Russian], Énergiya (1967).
5. I. G. Nekrashevich and I. A. Bakuto, in: Nauchnykh Trudov FTI AN BSSR, Izd-vo AN BSSR, No. 2 (1955).
6. A. G. Goloveiko, Inzhen.-Fiz. Zh., 13, No. 2 (1967).
7. S. I. Anisimov et al., Zh. Tekh. Fiz., 36, No. 7 (1966).
8. Ya. B. Zel'dovich and Yu. P. Raizer, The Physics of Shock Waves and High-Temperature Hydrodynamic Phenomena [in Russian], Nauka (1966).
9. M. V. Afanas'eu and S. N. Kapel'yan, Bestsi AN BSSR, Ser. Fiz.-Tekhn., No. 2 (1965).
10. M. A. Sultanov and L. I. Kiselevskii, Teplofiz. Vys. Temp., 4, 40, 375 (1966).